Chapter 17

Mosaicing

Frédéric Gueth[1,2]

gueth@iram.fr

[1] Max Planck Institute für Radioastronomie, Auf dem Hügel 69, D-5300 Bonn, Germany

[2] IRAM, 300 rue de la piscine, F-38406 Saint-Martin-d'Hères, France

17.1 Introduction

For a single-field interferometric observation, the dirty map F is obtained by Fourier Transform of the observed visibilities. It is related to the actual sky brightness distribution I by:

$$F = D * (B \times I) + N \tag{17.1}$$

where D is the dirty beam, B the antenna primary beam, and N a noise distribution[1]. Hence, an interferometer only measures the product $B \times I$. B is a rapidly decreasing function, and it therefore limits the size of the region it is possible to map. Correcting for the primary beam attenuation (i.e. dividing the map by B) is possible, and necessary for a proper estimate of the flux densities, but it does not enlarge the field of view, because of the noise distribution strongly increasing with the distance to the map center after such a correction.

Due to the coupling between the receiver horn and the primary mirror of the antennas (see Chapter 1 by A. Greve), the primary beam B is, to a good approximation, a Gaussian. Its FWHM, proportional to the ratio of the wavelength λ to the antenna diameter $\mathcal{D}$, can therefore be used to quantify the field of view. Note that this size does not correspond to a clear cut of the map, but to the 50% attenuation level. Table 17.1 gives the resulting values for the Plateau de Bure interferometer, for different frequencies. To map regions more extended than the primary beam width, it is necessary to observe a *mosaic* of several

[1] In the following, we will assume an uniform noise rms, i.e. we do not take into account variation of the noise introduced by the imaging process (see Chapter 15 by S. Guilloteau).

Frequency (GHz)	Wavelength (mm)	Field of View ($''$)	Largest structure ($''$)
85	3.5	58	36
100	3.0	50	31
115	2.6	43	27
215	1.4	23	14
230	1.3	21.5	13
245	1.2	20	12

Table 17.1: Field of view of the Plateau de Bure interferometer (15 m dishes). The two groups of frequencies correspond to the two receivers that are currently available. The last column gives *rough estimates* of the size of the largest structure which can be observed.

adjacent fields. Clearly, due to the gaussian-shape of the primary beam attenuation, these fields have to strongly overlap to ensure a roughly uniform sensitivity over the whole mapped region.

A further complication arises from the lack of the short-spacings information in the interferometer data set. Due to their diameter, the antennas cannot be put too close to each other, which results in a minimal measured baseline (24 m at the Plateau de Bure). Even if projection effects reduce the effective baselines, a central "hole" in the data distribution in the uv plane cannot be avoided. As a consequence, the extended structures (whose visibilities are confined in a small region in the uv plane) are filtered out. The largest structure it is possible to map with a single-field interferometric observation is thus even smaller than the field of view, and can be very roughly estimated by the ratio of the wavelength to the minimal baseline (Table 17.1).

17.2 Image formation in a mosaic

Some important mosaic properties can be understood by analyzing the combination of the data directly in the uv plane. This analysis was first proposed by [Ekers & Rots 1979]. The reader is also referred to [Cornwell 1989]. We consider a source with a brightness distribution $I(x, y)$, where x and y are two angular coordinates. The "true" visibility, i.e. the Fourier Transform of I, is noted $V(u, v)$. An interferometer baseline, with two identical antennas whose primary beam is $B(x, y)$, measures a visibility at a point (u, v) which may be written as:

$$V_{\rm mes}(u,v) = \int\!\!\int_{-\infty}^{+\infty} B(x,y)\, I(x,y)\, {\rm e}^{-2i\pi(ux+vy)}\, dx\, dy \tag{17.2}$$

If the observation is performed with a phase center in $(x = 0, y = 0)$ but with a pointing center in (x_p, y_p), the measured visibility (whose dependence on (x_p, y_p) is here explicitly indicated) is:

$$V_{\rm mes}(u,v,x_p,y_p) = \int\!\!\int_{-\infty}^{+\infty} B(x-x_p,y-y_p)\, I(x,y)\, {\rm e}^{-2i\pi(ux+vy)}\, dx\, dy \tag{17.3}$$

Using the symmetry properties of the primary beam B, this last relation can be rewritten:

$$V_{\rm mes}(u,v,x_p,y_p) = B(x_p,y_p) * \mathcal{F}(u,v,x_p,y_p) \tag{17.4}$$

where $*$ denotes a convolution product and the function $\mathcal{F}$ is defined as:

$$\mathcal{F}(u,v,x_p,y_p) = I(x_p,y_p)\, {\rm e}^{-2i\pi(ux_p+vy_p)} \tag{17.5}$$

Now, let's imagine an ideal "on-the-fly" mosaic experiment: for a given, fixed, (u, v) point, the pointing direction is continuously modified, and the variation of the visibility $V_{\rm mes}$ with $(x_p,\ y_p)$ can thus be monitored. The Fourier Transform of these data with respect to (x_p, y_p) would give (from Eq. 17.4):

$$\left[{\rm FT_p}\left(V_{\rm mes}\right)\right](u_p,v_p) = T(u_p,v_p)\, V(u+u_p,v+v_p) \tag{17.6}$$

where:

- $\mathrm{FT_p}$ denotes the Fourier Transform with respect to (x_p, y_p).
- (u_p, v_p) are the conjugate variables to (x_p, y_p).
- $[\mathrm{FT_p}(V_{\mathrm{mes}})]\,(u_p, v_p)$ is the Fourier Transform of the observations.
- $T(u_p, v_p)$ is the Fourier Transform of the primary beam $B(x_p, y_p)$. T is thus the transfer function of each antenna. For a dish of diameter $\mathcal{D}$, $T(u_p, v_p) = 0$ if $(u_p^2 + v_p^2)^{1/2} > \mathcal{D}/\lambda$.
- $V(u + u_p, v + v_p)$ is the Fourier Transform of $\mathcal{F}(u, v, x_p, y_p)$ with respect to (x_p, y_p). Indeed, $\mathcal{F}$ is the product of the sky brightness distribution (whose Fourier Transform is V) by a phase term (see Eq. 17.5). Hence, its Fourier Transform is V taken at a shifted point.

For $\sqrt{u_p^2 + v_p^2} < \mathcal{D}/\lambda$, we can thus derive:

$$V(u + u_p, v + v_p) = \frac{[\mathrm{FT_p}(V_{\mathrm{mes}})]\,(u_p, v_p)}{T(u_p, v_p)} \tag{17.7}$$

This relation illustrates an important property of the experiment we have considered. The observations were performed at a given (u, v) point but with a varying pointing direction. Eq. 17.7 shows that is possible to derive from this data set the visibility $V(u + u_p, v + v_p)$ at all (u_p, v_p) which verify $(u_p^2 + v_p^2)^{1/2} < \mathcal{D}/\lambda$. In other terms, the measurements have been done at (u, v) but the redundancy of the observations allows to compute (through a Fourier Transform and a division by the antenna transfer function) the source visibility at all the points of a disk of radius $\mathcal{D}/\lambda$, centered in (u, v).

Interpretation

In very pictorial terms, one can say that the adjacent pointings reinforce each other and thereby yield an estimate of the source visibility at unmeasured points. Note however that the resulting image quality is not going to be drastically increased: more information can be extracted from the data, but a much more extended region has now to be mapped[2]. The redundancy of the observations has only allowed to rearrange the information in the uv-plane. This is nevertheless extremely important, as e.g. it allows to estimate part of the missing short-spacings (see below).

How is it possible to recover unmeasured spacings in the uv-plane? It is actually obvious that two antennas of diameter $\mathcal{D}$, separated by a distance $\mathcal{B}$, are sensitive to all the baselines ranging from $\mathcal{B} - \mathcal{D}$ to $\mathcal{B} + \mathcal{D}$. The measured visibility is therefore an average of all these baselines: V_{mes} is actually the convolution of the "true" visibility by the transfer function of the antennas. This is shown by the Fourier Transform of Eq. 17.2, which gives: $V_{\mathrm{mes}} = T * V$. Now, if the pointing center and the phase center differ, a phase gradient is introduced across the antenna apertures, which means that the transfer function is affected by a phase term. Indeed, the Fourier Transform of Eq. 17.3 yields:

$$V_{\mathrm{mes}}(u, v) = \left[T(u, v)\,\mathrm{e}^{-2i\pi(ux_p + vy_p)}\right] * V(u, v) \tag{17.8}$$

Hence, the measured visibilities are (still) a linear combination of the "true" visibilities. Measurements performed in various directions (x_p, y_p) give many such linear combinations. One can thus expect to derive from this linear system the initial visibilities, in the baseline range from $\mathcal{B} - \mathcal{D}$ to $\mathcal{B} + \mathcal{D}$. Eq. 17.7 just shows that a Fourier Transform allows to do that operation.

Field spacing in a mosaic

In the above analysis, a continuous drift of the pointing direction was considered. However, the same results can be reached in the case of a limited number of pointings, provided that classical sampling theorems are fulfilled. We want to compute the visibility in a finite domain, which extends up to $\pm\mathcal{D}/\lambda$ around the nominal (u, v) point, and therefore the pointing centers have to be separated by an angle of

[2] We have considered observations in different directions, performed with the same uv-coverage. The analysis presented here shows that such an experiment is somehow equivalent to a single observation of the whole source, but with a denser uv-coverage.

$\lambda/2\mathcal{D}$ radians (see [Cornwell 1988]). In practice, the (gaussian) transfer function of the millimeter dishes drops so fast that one can use without consequences a slightly broader, more convenient, sampling, equal to half the primary beam width (i.e. $1.2\,\lambda/2\mathcal{D}$).

Mosaics and short-spacings

As with any other measured point in the uv plane, it is possible to derive visibilities in a small region (a disk of diameter $\mathcal{D}/\lambda$) around the shortest measured baseline. This is the meaning of the statement that mosaics can recover part of the short-spacings information: a mosaic will include (u, v) points corresponding to the shortest baseline minus $\mathcal{D}/\lambda$.

In practice, however, things are more complex. First, we have to deal with noisy data. As a consequence, it is not possible to expect a gain of $\mathcal{D}/\lambda$: the transfer function T which is used in Eq. 17.7 is strongly decreasing, and thus signal-to-noise ratio limits the gain in the uv plane to a smaller value, typically $\mathcal{D}/2\lambda$ ([Cornwell 1988]). This is still a very useful gain: for the Plateau de Bure interferometer, this corresponds to a distance in the uv plane of 7.5 m/λ, while the shortest (unprojected) baseline is 24 m/λ. Secondly, the analysis described above would be rather difficult to implement with real observations, which have a limited number of pointing centers and different uv-coverages. Instead, one prefers to combine the observed fields to directly reconstruct the sky brightness distribution. The resulting image should include the information arising from the redundancy of the adjacent fields, among them part of the short-spacings. However, the complexity of the reconstruction and deconvolution algorithms that have to be used precludes any detailed mathematical analysis of the structures in the maps. For instance, the (unavoidable) deconvolution of the image can also be interpreted as an interpolation process in the uv plane (see [Schwarz 1978] for the case of the CLEAN algorithm) and its effects can thus hardly be distinguish from the intrinsic determination of unmeasured visibilities that occur when mosaicing.

17.3 Mosaicing in practice

Observation and calibration

The observation of a mosaic with the Plateau de Bure interferometer and the calibration of the data do not present any specific difficulties. We just mention here a few practical remarks:

- As shown in the previous paragraph, the optimal spacing between adjacent fields is half the half-power primary beam width. Larger separations can be used (e.g. to map larger field of view in the same amount of time) but the image reconstruction is not optimal in that case. Since observations are performed with dual-channel receivers (operating at 1.3 and 3 mm), the field spacing has to be chosen for one of the frequencies. Consequently, the mosaic observed at the other frequency is either under- or oversampled.

- Even if this is not formally required by the reconstruction and deconvolution algorithm described in the following section, it seems quite important to ensure similar observing conditions for all the pointing centers. Ideally, one wants the same noise level in each field – so that the noise in the final image is uniform – and the same uv-coverage – to avoid strong discrepancies (in terms of angular resolution and image artifacts) between the different parts of the mosaic. In practice, the fields are observed in a track-sharing mode, i.e. in a loop with a few minutes integration time per pointing direction: hence, atmospheric conditions and uv-coverage are similar for all the fields.

- In most cases, a mosaic is not observed during an amount of time significantly larger than normal projects. As the observing time is shared between the different pointing centers, the sensitivity of each individual field is thus smaller than what would have been achieved with normal single-field observations. Note however that the sensitivity is further increased in the mosaic, thanks to the strong overlap between the adjacent fields (see below, Fig. 17.1).

- The number of fields, and therefore the size of the mosaic, is limited by the requirement to get good enough sensitivity and uv-coverage for all the fields in a reasonable amount of observing time. The

current observing mode used at the Plateau de Bure limits the maximum number of fields to about 20. Observing more fields is in principle possible, but would require (much) more observing time and/or an other approach (e.g. mosaic of several mosaics). Note that in any case, the *uv*-coverage obtained for each field is sparse as compared to normal synthesis observations. Finally, a potential practical limitation is the disk and memory sizes of the computers, as mosaicing requires to handle very large data cubes.

- The calibration of the data, including the atmospheric phase correction, is strictly identical with any other observation performed with the Plateau de Bure interferometer, as only the observations of the calibrators (quasars) are used. At the end of the calibration process, a *uv* table and then a dirty map are computed for each pointing center.

Mosaic reconstruction

The point is now to reconstruct a mosaic from the observations of each field, in an optimal way in terms of signal-to-noise ratio. For the time being, let's forget the effects of the convolution by the dirty beam. Each field i can then be written: $F_i = B_i \times I + N_i$, where B_i is the primary beam of the interferometer, centered in a different direction for each observation i, and N_i is the corresponding noise distribution. In practice, the same phase center (i.e. the same coordinate system) is used for all the fields.

Hence, the mosaic observations can be described as several measurements of the same unknown quantity I, each one being affected by a weighting factor B_i. This is a classical mathematical problem: the best estimate J of I, in the least-square sense, is given by:

$$J = \frac{\sum_i \frac{B_i}{\sigma_i^2} F_i}{\sum_i \frac{B_i^2}{\sigma_i^2}} \tag{17.9}$$

where the sum includes all the observed fields and σ_i is the rms of the noise distribution N_i. (Note that in Eq. 17.9 as well as in the following equations, σ_i is a number while other letters denote two-dimensional distributions).

Linear vs. non-linear mosaicing

The problem which remains to be address is the deconvolution of the mosaic. This is actually the main difficulty of mosaic interferometric observations. Two different approaches have been proposed (e.g. [Cornwell 1993]):

- *Linear mosaicing:* each field is deconvolved using classical techniques, and a mosaic is reconstructed afterwards with the clean images, using Eq. 17.9.

- *Non-linear mosaicing:* a joint deconvolution of all the fields is performed, i.e. the deconvolution is performed after the mosaic reconstruction.

The deconvolution algorithms are highly non-linear, and the two methods are therefore not equivalent. The first one is straightforward to implement, but the non-linear mosaicing algorithms give much better results. Indeed, the combination of the adjacent fields in a mosaic allows to estimate visibilities which were not observed (see previous paragraph), it allows to remove sidelobes in the whole mapped area, and it increases the sensitivity in the (large) overlapping regions: these effects make the deconvolution much more efficient.

Non-linear deconvolution methods based on the Maximum Entropy Method (`MEM`) have been proposed by [Cornwell 1988] and [Sault et al 1996]. As CLEAN deconvolutions are usually applied on Plateau de Bure data, a CLEAN-based method adapted to the case of the mosaics has been developed. The initial idea was proposed by F. Viallefond (DEMIRM, Paris) and S. Guilloteau (IRAM), and the algorithm is now implemented in the MAPPING software.

17.4 A CLEAN-based algorithm for mosaic deconvolution

The dirty mosaic

The dirty maps of each field i are computed with the same phase center (i.e. the same coordinate system) and can thus be written:

$$F_i = D_i * (B_i \times I) + N_i \tag{17.10}$$

Note that the dirty beams D_i are *a priori* different for each pointing center, because the uv-coverages, even if similar, are slightly different. The dirty mosaic J can then be constructed according to Eq. 17.9:

$$J = \frac{\sum_i \frac{B_i}{\sigma_i^2} F_i}{\sum_i \frac{B_i^2}{\sigma_i^2}} = \frac{\sum_i B_i \, \sigma_i^{-2} \left[D_i * (B_i \times I) + N_i \right]}{\sum_i B_i^2 \, \sigma_i^{-2}} \tag{17.11}$$

This relation is homogeneous to the sky brightness distribution I: the mosaic is corrected for the primary beams attenuation. In practice, a slightly modified mosaic is computed, in order to avoid noise propagation (it makes no sense to add to the center of a field noise coming from the external, attenuated regions of an adjacent field). For that purpose, the primary beams used to construct the mosaic are truncated to some value, typically 10 to 30% of the maximum. The mosaic is thus defined by:

$$J = \frac{\sum_i \frac{B_i^t}{\sigma_i^2} F_i}{\sum_i \frac{B_i^{t2}}{\sigma_i^2}} = \frac{\sum_i B_i^t \, \sigma_i^{-2} \left[D_i * (B_i \times I) + N_i \right]}{\sum_i B_i^{t2} \, \sigma_i^{-2}} \tag{17.12}$$

where B_i^t denotes the truncated primary beam of the field i. This relation is the "measurement equation" of a mosaic, connecting the observed quantity J to the sky brightness distribution I (Eq. 17.1 was the measurement equation of a single-field observation).

Noise distribution

Due to the correction for the primary beams attenuation, the noise distribution in a mosaic is not uniform. From Eq. 17.12, it can be written:

$$N = \frac{\sum_i B_i^t \, \sigma_i^{-2} \, N_i}{\sum_i B_i^{t2} \, \sigma_i^{-2}} \tag{17.13}$$

Accordingly, the noise rms σ_J depends on the position and is given by:

$$\sigma_J = \frac{\sqrt{\sum_i B_i^{t2} \, \sigma_i^{-2}}}{\sum_i B_i^{t2} \, \sigma_i^{-2}} = \frac{1}{\sqrt{\sum_i B_i^{t2} \, \sigma_i^{-2}}} \tag{17.14}$$

Hence, the noise strongly increases at the edges of the mosaic, and the resulting image has thus to be truncated (see Fig. 17.1). The non-uniformity of the noise level with the position makes it impossible to use classical CLEAN methods to deconvolve the mosaic: the risk to identify a noise peak as a CLEAN component would be too important. It is thus necessary to identify the CLEAN components on another distribution. For that purpose, the "signal-to-noise" distribution is computed:

$$H = \frac{J}{\sigma_J} = \frac{\sum_i B_i^t \, \sigma_i^{-2} \, F_i}{\sqrt{\sum_i B_i^{t2} \, \sigma_i^{-2}}}$$

$$\text{i.e. :} \qquad H = \frac{\sum_i B_i^t \, \sigma_i^{-2} \left[D_i * (B_i \times I) + N_i \right]}{\sqrt{\sum_i B_i^{t2} \, \sigma_i^{-2}}} \tag{17.15}$$

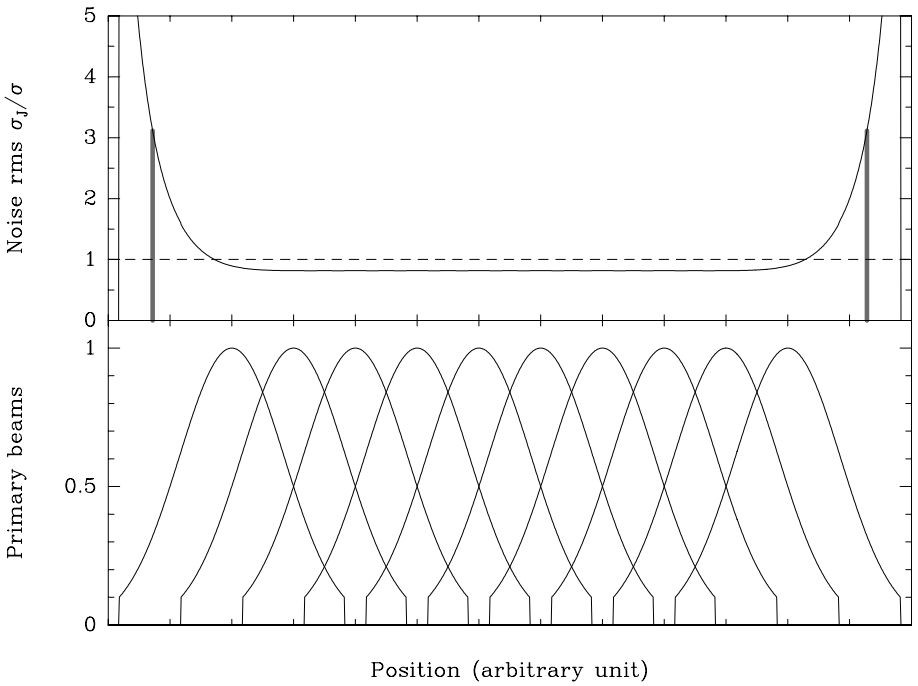

Figure 17.1: One-dimensional mosaic of 10 half-power overlapping fields, with identical noise level σ. Lower panel: Normalized primary beams, truncated to $\mathrm{B_{min}} = 0.1$. Upper panel: Resulting noise distribution (Eq. 17.14). The noise rms in the mosaic is roughly constant, about 20% lower than the noise of each individual field, but strongly increases at the edges. The two thick vertical lines indicate the truncation of the mosaic done by the algorithm at $\sigma_J = \sigma/\sqrt{\mathrm{B_{min}}}$.

Deconvolution algorithm

The main idea of the algorithm is to iteratively find the *positions* of the CLEAN components on H, and then to correct the mosaic J. The initial distributions J_0 and H_0 are computed from the observations and the truncated primary beams, using Eqs. 17.12 and 17.15. The following operations have then to be performed at each iteration k:

1. Find the position (x_k, y_k) of the maximum of H.
2. Find the value j_k of J at the position (x_k, y_k), whether it is the maximum of J or not.
3. Remove from J the contribution of a point-like source of intensity γj_k, located at (x_k, y_k) (γ is the loop gain, as in the normal CLEAN algorithm):

$$J_k = J_{k-1} - \frac{\sum_i B_i^t \, \sigma_i^{-2} \left[D_i * \left[\gamma \, j_k \, B_i(x_k, y_k) \, \delta(x_k, y_k) \right] \right]}{\sum_i B_i^{t^2} \, \sigma_i^{-2}} \tag{17.16}$$

   $\delta(x_k, y_k)$ denotes a Dirac peak located at (x_k, y_k).

4. Do the same for H: remove the contribution of a point-like source of intensity γj_k, located at (x_k, y_k):

$$H_k = H_{k-1} - \frac{\sum_i B_i^t \, \sigma_i^{-2} \left[D_i * \left[\gamma \, j_k \, B_i(x_k, y_k) \, \delta(x_k, y_k) \right] \right]}{\sqrt{\sum_i B_i^{t^2} \, \sigma_i^{-2}}} \tag{17.17}$$

   Note that in the two last relations, the CLEAN component is multiplied by the true, not truncated, primary beam (taken at the (x_k, y_k) position).

After $k_{\max}$ iterations, the mosaic J can thus be written:

$$J = \frac{\sum_i B_i^t \, \sigma_i^{-2} \left[D_i * \left(B_i \times \left[\sum_{k=1}^{k_{\max}} \gamma \, j_k \, \delta(x_k, y_k) \right] \right) \right]}{\sum_i B_i^{t2} \sigma_i^{-2}} + J_{k_{\max}} \tag{17.18}$$

Enough iterations have to be performed to ensure that the residual $H_{k_{\max}}$ is smaller than some user-specified threshold (typically 1 to 3). The comparison between Eqs. 17.12 and 17.18 shows that, within the noise, the sum of the CLEAN components can be identified with the sky brightness distribution I. As with the normal CLEAN algorithm, the final clean image is then reconstructed as:

$$M = C * \left[\sum_{k=1}^{k_{\max}} \gamma \, j_k \, \delta(x_k, y_k) \right] + J_{k_{\max}} \tag{17.19}$$

where C is the chosen clean beam. Note that the algorithm takes into account the dirty beams being different for each field, but the restoration is done using a single clean beam, which implicitly assumes that the dirty beams have similar widths. In practice, the observing mode of mosaics with the Plateau de Bure interferometer yields similar uv-coverages, and therefore similar dirty beams, for all the fields.

The modified CLEAN algorithms proposed e.g. by [Clark 1980] or [Steer et al. 1984] can be similarly adapted to handle mosaics, the main idea being to identify CLEAN components on H and to correct J. Note however that the multi-resolution CLEAN [Wakker & Schwartz 1988] cannot be directly adapted, as it relies on a linear measurement equation, which is not the case for a mosaic.

The MAPPING software

MAPPING is a superset of the GRAPHIC software, which has been developed to allow more sophisticated deconvolutions to be performed. For instance, it allows to choose a support for the deconvolution (clean window) or to monitor the results of the deconvolution after each iteration. Several enhancements of CLEAN (e.g. multi-resolution CLEAN) as well as the `WIPE` algorithm (see [Lannes et al. 1997]) are also available. The deconvolution of a mosaic has to be done with MAPPING. The implemented algorithm assumes that the noise levels in each field are similar (i.e. $\forall i \; \sigma_i = \sigma$), which is a reasonable hypothesis for Plateau de Bure observations. In that case, the equations of the previous paragraphs are slightly simplified: J is independent from σ, and H can be written as the ratio H'/σ, where H' is independent from σ and is used in practice to localize the CLEAN components.

We refer to the *Mapping Cookbook* for a description of the MAPPING software. To deconvolve mosaics, the following steps are performed:

- Create a uv table for each observed field. Then, run the `UV_MAP` task to compute a dirty map and a dirty beam for each field, with the *same* phase center (variable `UV_SHIFT = YES`).
- The task `MAKE_MOSAIC` is used to combine the fields to construct a dirty mosaic. Two parameters have to be supplied: the width and the truncation level $B_{\min}$ of the primary beams. Three images are produced: the dirty mosaic[3] (yourfile.lmv), all the dirty beams written in the same file (yourfile.beam), and a file describing the positions and sizes of the primary beams (yourfile.lobe). The dirty maps and beams of each individual field are no longer used after this step and can thus be removed if necessary.
- The data have to be loaded into the MAPPING buffers. This is done by the `READ DIRTY yourfile.lmv`, `READ BEAM yourfile.beam`, and `READ PRIMARY yourfile.lobe` commands. The latter automatically switches on the mosaic mode of MAPPING (the prompt is now `MOSAIC>`). From now, the deconvolution commands `HOGBOM`, `CLARK` and `SDI` (for Steer-Dewdney-Ito) can be used and will apply the algorithm described above. Use the command `MOSAIC` to switch on or off the mosaic mode if necessary.

[3] More precisely, this file contains the non normalized mosaic $\Sigma B_i^t \times F_i$. The proper normalization (see Eq. 17.12) is further done by the deconvolution procedures.

- The clean beam of the final image can be specified by the user (variables `MAJOR` and `MINOR`). Otherwise, the clean beam computed from the first field is used. To check if there are differences between the various dirty beams, just use the `FIT` i command, which computes the clean beam for the ith field.

- The deconvolution uses the same parameters as a classical CLEAN: support, loop gain, maximal number of iterations, maximal value of the final residual, etc.

- In addition, two other parameters, `SEARCH_W` and `RESTORE_W`, can be supplied. Due to the strong increase of the noise at its edges, the mosaic has to be truncated above some value of σ_J, and these two variables are used to define this truncation level, in terms of $(\sigma_J/\sigma)^{-2}$. More precisely, `SEARCH_W` indicates the limit above which CLEAN components have not to be searched, while `RESTORE_W` indicates the limit above which the clean image is not reconstructed. Default values of these two parameters (both equal to $B_{\min}$) are strongly recommended. The corresponding truncation is shown in Fig. 17.1.

Tests of the method

Several tests of the method described in this paragraph have been performed, either with observations (including the comparison of independent mosaics from the same source) or with simulations. They show that very satisfactory results can be achieved with typical Plateau de Bure observations. Interestingly, deconvolution of the same data set using `MEM` (e.g. the task `VTESS` in `AIPS`) seems to give worse results: this is most probably related to the limited uv-coverage obtained with the Plateau de Bure interferometer, as compared to typical VLA observations (`MEM` is known to be vulnerable when there is a relatively small number of visibilities).

17.5 Artifacts and instrumental effects

The behaviour of the mosaicing algorithm towards deconvolution artifacts and/or instrumental effects can be studied by the means of simulations of the whole mosaicing process. The simulations presented below were computed with several models of sky brightness distributions. uv-coverages of real observations were used (4–antennas CD configuration of a source of declination $\delta = 68°$). No noise has been added to the simulations shown in the figures, so that pure instrumental effects can directly be seen.

Stripes

A well-known instability of the CLEAN algorithm is the formation of stripes during the deconvolution of extended structures. After the dirty beam has been subtracted from the peak of a broad feature, the negative sidelobes of the beam are showing up as positive peaks. The next iterations of the algorithm will then identify these artificial peaks as CLEAN components. A regular separation between the CLEAN components is thereby introduced and the resulting map shows ripples or stripes. [Steer et al. 1984] proposed an enhancement of CLEAN (implemented as the command `SDI` in MAPPING) which prevents such coherent errors: the CLEAN components are identified and removed in groups. As mosaics are precisely observed to map extended sources, the formation of stripes can *a priori* be expected. Indeed, the algorithm described in the previous paragraph presents this instability. Fig. 17.2 shows an example of the formation of such ripples. To make them appear so clearly, an unrealistic loop gain ($\gamma = 1$) was used. Interestingly, the algorithm of [Steer et al. 1984], adapted to the mosaics, does not result in these stripes, even with the same loop gain. It seems thus to be a very efficient solution to get rid of this problem, if it should occur. Note however that more realistic simulations, including noise and deconvolved with normal loop gain, do not show stripes formation. This kind of artifacts seems thus not to play a significant role in the image quality, for the noise and contrast range of typical Plateau de Bure observations. In practice, they are never observed.

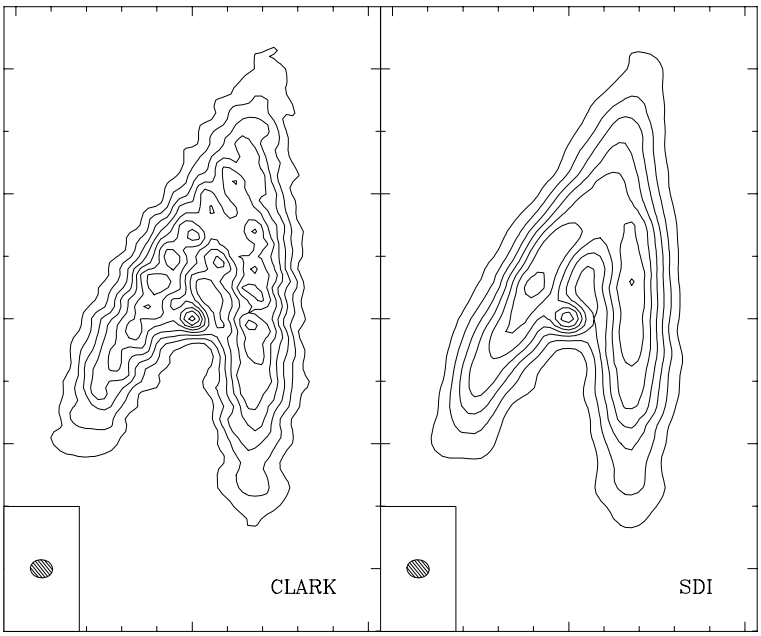

Figure 17.2: Mosaic deconvolved with the `CLARK` or `SDI` algorithms. Deconvolution parameters were identical (with a loop gain = 1) and contours are the same in the two images. The formation of stripes does not occur when using the `SDI` algorithm.

Short-spacings

The mosaicing technique allows, at least in theory, to recover part of the short-spacings information (see Section 17.2). In practice, however, the lack of the short-spacings cannot be fully compensated, and thus still introduces severe artifacts in the reconstructed images. The mosaic case is actually more complex than the single-field case, because the most extended structures are filtered out in each field, thus introducing a lack of information on an *intermediate* scale as compared to the size of the mosaic. As a consequence, a very extended emission can be split into several pieces, each one having roughly the size of the primary beam. This effect can be very well seen on the simulation presented in Fig. 17.3. To correct for this problem, it is necessary to add the short-spacings informations (deduced typically from single-dish observations) to the interferometric data set. Note however that the effects of the missing short-spacings on the reconstructed mosaic strongly depend on the actual *uv*-coverage of the observations, as well as on the size and morphology of the source: the artifacts can be small or negligible if the observed emission is confined into reasonably small regions. From this point of view, the example shown in Fig. 17.3 represents the worst case.

In any case, CLEAN is known to be not optimal to deconvolve smooth, extended structures. In order to partially alleviate this problem and the effects of the missing short-spacings, [Wakker & Schwartz 1988] proposed an enhanced algorithm, the so-called multi-resolution CLEAN: deconvolutions are performed at low- and high-resolution, and the results are combined to reconstruct an image which then accounts for the extended structures much better than in the case of a classical CLEAN deconvolution. As already quoted before, this algorithm cannot be applied to a mosaic, because it relies on a linear measurement equation. A multi-resolution CLEAN adapted to mosaics has however been developed ([Gueth 1997]) and is implemented in MAPPING. This method will not be described here.

Pointing errors

Pointing errors during the observations can of course strongly affect the images obtained by mosaicing. The rms of the pointing errors of the antennas of the Plateau de Bure interferometer is about $3''$. By comparison, the primary beam size at 230 GHz is $\sim 22''$ (Table 17.1). The pointing errors are difficult to model precisely: they are different for each antenna, random errors as well as slow drifts occur, the

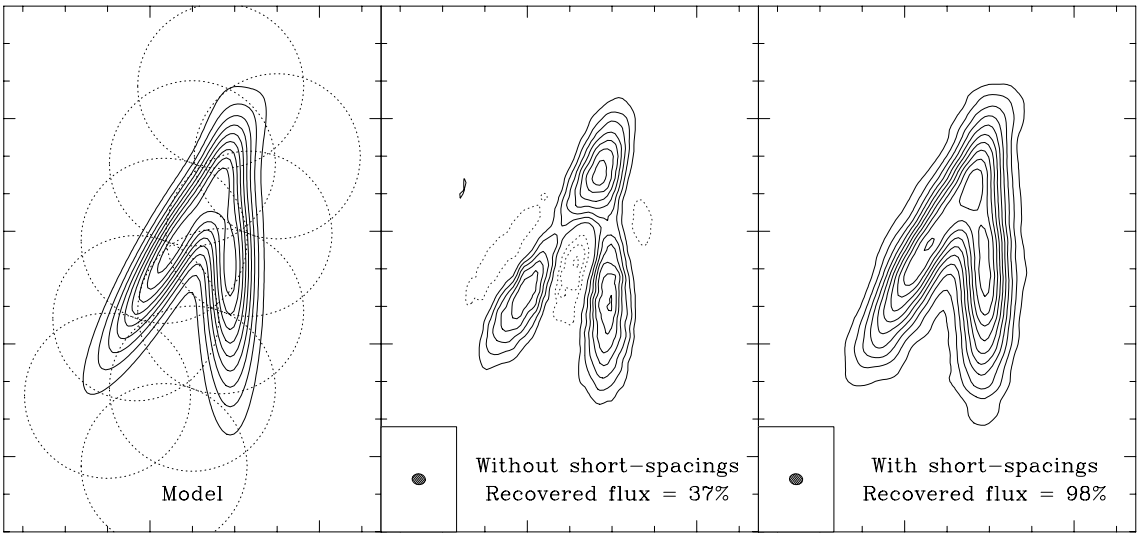

Figure 17.3: Left: Initial model of a very extended sky brightness distribution. Dotted circles indicate the primary beams of the simulated observation. Middle: Reconstructed mosaic, without the short-spacings information. Right: Reconstructed mosaic, with the short-spacings information. The contours are the same in the two simulated observations.

amplitude calibration partially corrects them, etc. A complete simulation should therefore introduce pointing errors during the calculation of each visibility. For typical Plateau de Bure observations, such a detailed modeling is probably not necessary, as the final image quality is dominated by deconvolution artifacts. To get a first guess of the influence of pointing errors, less realistic simulations were thus performed, in which each field is shifted as a whole by a (random) quantity. Such a systematic effect most probably maximizes the distortions introduced in the images. (Note that for a single field, the source would simply be observed at a shifted position in such a simulation. For a mosaic, the artifacts are different, because each individual field has a different, random pointing error. See [Cornwell 1987] for a simplified analysis in terms of visibilities. Figure 17.4 presents typical reconstructed mosaics for different rms of the pointing errors of the Plateau de Bure antennas. Obviously, the larger the pointing error, the worse the image quality. With a pointing error rms of $3''$, reasonably correct mosaics can be reconstructed even at 230 GHz. Clearly, care to the pointing accuracy has however to be exercised when mosaicing at the highest frequencies.

17.6 Concluding remarks

Mosaic observations are now routinely performed with the Plateau de Bure interferometer, at both λ 3 mm and λ 1.3 mm. It has proven to be a very efficient method to map extended sources, including using the most extended configuration of the array. The number of fields are usually ≤ 6, but can be more important in some cases: as of the date of writing, the largest observed mosaic has 20 fields. Data processing requires a few more operations than normal observations, but does not present any specific difficulties. Reconstruction and deconvolution algorithms are available in the MAPPING software.

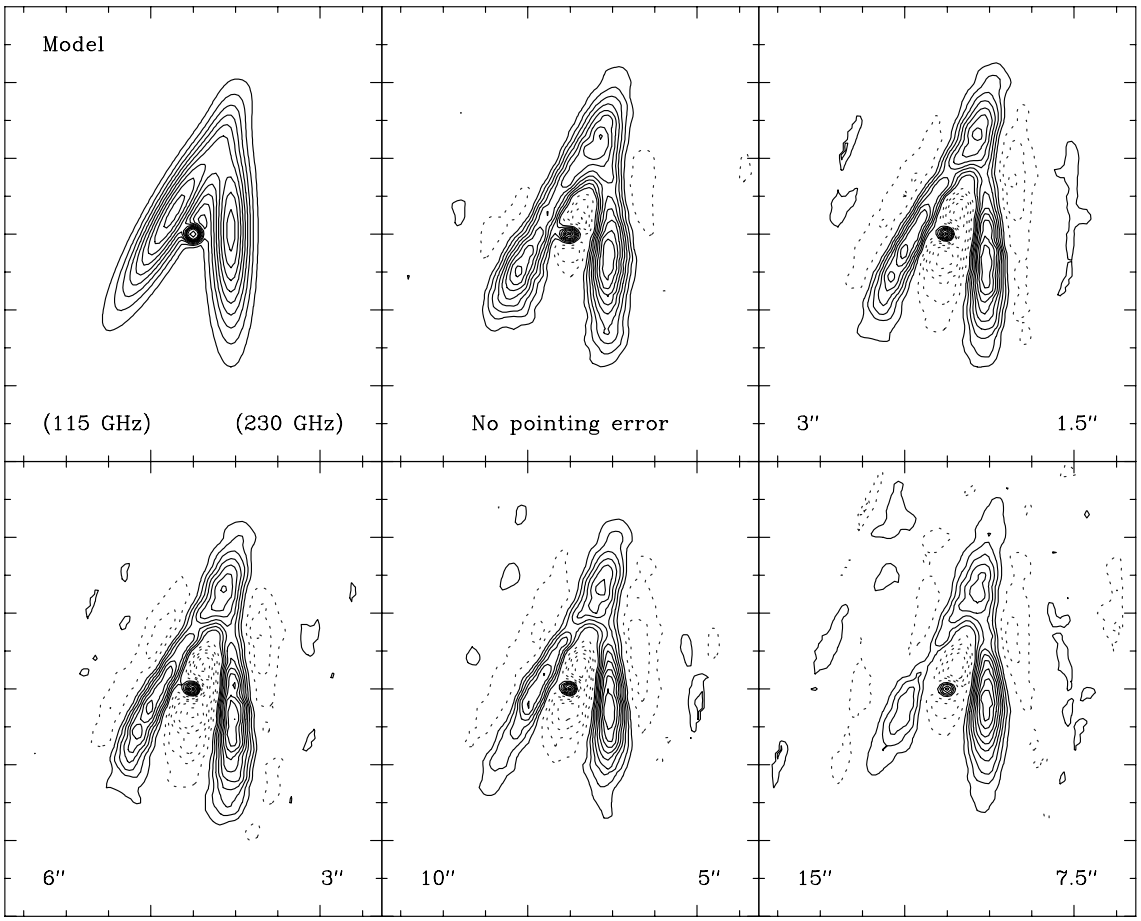

Figure 17.4: Simulations of a 10–fields mosaic observed with the Plateau de Bure interferometer. Each field is affected by a pointing error (see text). The corresponding rms are indicated in the lower left (observations performed at 115 GHz) and lower right (230 GHz) corners of each panel.